

A 9 Å single particle reconstruction from CCD captured images on a 200 kV electron cryomicroscope

Christopher R. Booth,^a Wen Jiang,^b Matthew L. Baker,^b Z. Hong Zhou,^{a,c}
Steven J. Ludtke,^b and Wah Chiu^{a,b,*}

^a Program in Structural and Computational Biology and Molecular Biophysics, Baylor College of Medicine, Houston, TX 77030, USA

^b National Center for Macromolecular Imaging, Verna and Marrs McLean Department of Biochemistry and Molecular biology, Baylor College of Medicine, Houston, TX 77030, USA

^c Department of Pathology and Laboratory Medicine, The University of Texas Health Science Center at Houston Medical School, 6431 Fannin, Houston, TX 77030, USA

Received 12 November 2003, and in revised form 3 February 2004

Available online 16 March 2004

Abstract

Sub-nanometer resolution structure determination is becoming a common practice in electron cryomicroscopy of macromolecular assemblies. The data for these studies have until now been collected on photographic film. Using cytoplasmic polyhedrosis virus (CPV), a previously determined structure, as a test specimen, we show the feasibility of obtaining a 9 Å structure from images acquired from a 4 k × 4 k Gatan CCD on a 200 kV electron cryomicroscope. The match of the α -helices in the protein components of the CPV with the previous structure of the same virus validates the suitability of this type of camera as the recording media targeted for single particle reconstructions at sub-nanometer resolution.

© 2004 Elsevier Inc. All rights reserved.

Keywords: CCD; Electron cryomicroscopy; Cryo-EM; Structure; Cytoplasmic polyhedrosis virus; MTF

1. Introduction

In recent years it has become feasible to solve a structure at sub-nanometer resolution by single particle reconstruction techniques (see review: Zhou and Chiu, 2003). Using a 1 k × 1 k charge coupled device (CCD) camera, images of protein crystals beyond 4 Å on a 400 kV cryomicroscope have been recorded (Sherman and Chiu, 1997). However, the usage of a CCD for image acquisition of ice embedded specimens for single particle reconstructions has not been considered practical. This is largely due to three major limitations of the previous generations of CCD cameras. When an object is imaged at a comparable sampling (Å/pixel) on CCD and film, film has 30 times more pixels than a 2 k × 2 k CCD camera, but only 8 times more pixels than an 4 k × 4 k CCD camera. The second limitation is attenu-

ation of high resolution information due to the point spread function of the CCD camera system, including effects of the scintillator and the fiber optics. Third, increasing the electron accelerating voltage makes the effect of the point spread function worse (Downing and Hendrickson, 1999; Meyer and Kirkland, 2000).

Recently, with a 4 k × 4 k Gatan CCD camera on a 120 kV electron cryomicroscope, structural data to 15 Å from pyruvate dehydrogenase was reported (Zhang et al., 2003). However, the suitability of using this new generation of CCD camera for single particle reconstructions targeted at sub-nanometer resolution has not been documented. In this article, we characterize the Gatan US4000 CCD camera and demonstrate its applicability in sub-nanometer resolution structure determination. We performed a single particle reconstruction of cytoplasmic polyhedrosis virus (CPV) to 9 Å with a JEOL2010F electron cryomicroscope operated at 200 kV. CPV was chosen as the test specimen due to the recently obtained structure to 8 Å resolution from

* Corresponding author. Fax: 1-713-798-1625.

E-mail address: wah@bcm.tmc.edu (W. Chiu).

electron cryomicroscopy data collected on film and subsequently digitized by scanning (Zhou et al., 2003).

2. Materials and methods

2.1. Electron cryomicroscopy

All images were acquired using a JEOL2010F electron microscope (JEOL, Tokyo Japan) with a field emission gun operated at 200 kV. This microscope was equipped with the JEOL telemicroscopy software package (FastEM) (JEOL USA, Peabody MA), a Gatan Model 626 cryostage (Gatan, Pleasanton CA) and a Gatan US4000 4k × 4k CCD camera (Gatan, Pleasanton CA). FastEM is JEOL's computer controlled microscopy software package, which can control stage motion, aperture adjustment and low dose imaging (<http://www.jeol.com/tem/temprods/fastem.html>). Although this software does not provide any automation of data collection, it is essential for our experimental protocol. All images were acquired on the CCD camera unless otherwise noted.

2.2. CCD characterization

The magnification of the CCD camera was calibrated by calculating the Fourier transform of an image of graphitized carbon (Electron Microscopy Services, Ft. Washington PA) with diffraction peaks at 1/3.44 Å⁻¹. From the distance, in pixels, that these peaks were located from the origin in the Fourier space, the increase of the effective magnification on the CCD camera over that of film was determined to be a factor of 1.38. In this estimate, we assumed the pixel size of the camera to be 15 μm, as specified by the manufacturer.

The MTF of the CCD camera was estimated using the method of de Ruijter and Weiss (de Ruijter and Weiss, 1992). Briefly, the CCD was evenly illuminated with the electron beam without any specimen. Images were collected across a range of dosages, ranging from 450 to 1500 counts/pixel. These values correspond to a specimen dose, ~9–30 electrons/Å², typically used for imaging ice embedded single particles. The pixel intensities of these images should be uncorrelated noise. The autocorrelation function of these images should only have a peak at zero, and a deviation from this result provides an estimate for the point spread function of the CCD. Using this point spread function estimate, the MTF is calculated as follows:

$$\text{MTF}(s, \theta) = \sqrt{F^{-1}[\text{ACF}(r, \phi)]},$$

$$\text{MTF}(s) = \frac{1}{2\pi} \sum_{\theta=0}^{2\pi} \text{MTF}(s, \theta),$$

where $\text{ACF}(r, \phi)$ is the 2-D autocorrelation function of a sample free image, F^{-1} is the inverse Fourier trans-

form operator, and $\text{MTF}(s, \theta)$ and $\text{MTF}(s)$ are the 2-D and 1-D modulation transfer functions, respectively.

A comparison between detection on photographic film and on the CCD camera was made using amorphous carbon film (Electron Microscopy Services, Ft. Washington PA). Under low dose conditions at 60 000× microscope magnification, an area of thin amorphous carbon film was recorded respectively on Kodak SO163 film (developed in full strength D19 for 12 min at 20 °C) and on the CCD camera. The specimen dosage was held constant during data collection on both detectors. This was done for two reasons, the first of which is due to the inherent dose constraint of the biological specimen. Secondly, we have observed that for this range of dosages the signal-to-noise ratio (SNR) is proportional to the dosage on the specimen rather than on the detector (unpublished data). Prior to the image acquisition, the area of amorphous carbon film being imaged was exposed to a relatively high electron dose as the microscope was being aligned and the astigmatism was corrected. This was to ensure that the carbon film has a stable structure between exposures on film and CCD. For the data presented here, images were taken at a series of defocus settings ranging from 0.4 to 3.5 μm underfocus. For a given defocus, images were first acquired on CCD and then on film. Since the post-column magnification of the CCD camera is 1.38 and the pixel size of the CCD camera is 15 μm, a final sampling value of 1.81 Å/pixel at a microscope magnification of 60 000× was determined. Images recorded on photographic film were scanned on a Zeiss high resolution scanner (Z/I Imaging, Huntsville, Al) at a step size of 7 μm/pixel, giving a final sampling value of 1.17 Å/pixel at this magnification. The 2-D power spectrum of each image was estimated by incoherently averaging the 2-D Fourier transforms of these images. A 1-D power spectrum was calculated by rotationally averaging the 2-D power spectrum. Minima corresponding to the zeroes of the CTF are clearly observed. Since the signal is theoretically zero at these points, we assume that a smooth curve connecting these points can be used to estimate the background noise (Ludtke et al., 2001; Saad et al., 2001). From the power spectrum and the noise curve, the SNR as a function of spatial frequency could be calculated as follows,

$$\text{SNR}(s) = \frac{P(s) - N(s)}{N(s)},$$

where $\text{SNR}(s)$ is the signal-to-noise ratio, $P(s)$ is the 1-D power spectrum of the image and $N(s)$ is the noise function.

2.3. Virus purification and cryo-specimen preparation

Bombyx mori CPV was purified from the midguts of infected silk worms using a previously described

procedure (Zhou et al., 2003). Freshly isolated virus samples were flash frozen in liquid ethane on washed, glow discharged, and electron-beam irradiated quantifoil R2-1 holey carbon grids (Quantifoil Micro Tools GmbH, Jena Germany). Samples were then stored in liquid nitrogen until they could be transferred to the electron cryomicroscope for imaging.

2.4. JAMES (JEOL automated microscopy expert system)

JAMES is a custom software package developed in-house for automation of cryomicroscopy on JEOL microscopes (Booth, CR, unpublished). Briefly, this package coordinates the communication between the microscope, CCD camera and database (Ludtke et al., 2003) to eliminate the need to deal with multiple computers and software simultaneously during the data collection. JAMES has been designed to perform on-line, real-time data preprocessing and provide feedback on the quality of the images acquired during a microscopy session. In this study, JAMES performs semi-automated data collection, such as acquiring focal pairs and uploading them to the database along with relevant meta-data upon the operator's request. Using JAMES, 428 focal pairs from 6 grids were acquired over a 5 day period to complete this dataset (Table 1). 381 of these focal pairs were used in the final reconstruction (Table 1).

2.5. Imaging of ice embedded specimens

Virus particles were imaged on a JEOL2010F electron microscope operating at 200 kV. The microscope was operated at 83 100 \times effective magnification, corresponding to a pixel size of 1.81 Å/pixel, with a specimen dosage of approximately 12 e⁻/Å². Each specimen area was imaged two times, the first image relatively close to focus (0.8–2.5 μ m) and the second image slightly farther from focus (2.5–4.0 μ m). Each CCD frame was background subtracted and gain normalized before being saved or viewed (Aikens et al., 1989). Each frame was immediately uploaded to our database (Ludtke et al., 2003) along with other relevant metadata about the acquisition by the JAMES software package.

Table 1
Image collection and 3-D reconstruction statistics

Total number of grids Viewed	9
Number of grids used for data collection	6
Total number of focal pairs collected	428 (856 total)
Focal pairs with usable particles	381 (762 total)
Total number of unique particles	6603 (13 206 total)
Average number of unique particles/focal pair	17
Unique particles used in reconstruction	6465 (12 930 total)
Unique particles used in final reconstruction	5546

2.6. Preprocessing of CCD frames

Far from focus CCD frames were aligned to their close to focus counterparts using the *EMAN* software program *alignhuge* (Ludtke et al., 1999). After alignment, particles were automatically boxed out of the far from focus micrograph using the program *ethan* (Kivioja et al., 2000). The automatically generated boxes were checked for particles that were obviously overlapping, or partially outside the micrograph. Unsuitable particles were removed from the dataset using the *EMAN* program *boxer* (Ludtke et al., 1999). Close to focus micrographs were boxed out by applying the boxes from the far from focus micrograph to the close to focus micrograph using the *EMAN* program *batchboxer* (Ludtke et al., 1999). CTF parameters for each image were initially estimated using the *EMAN* software program *fitctf* (Ludtke et al., 1999; Ludtke et al., 2001). CTF parameters for each micrograph were checked and corrected manually, if necessary, using the *EMAN* program *ctfit* (Ludtke et al., 1999; Ludtke et al., 2001).

2.7. 3-D reconstruction

Boxed out particles and CTF parameters were provided to the semi-automated virus reconstruction package (SAVR) (Jiang et al., 2001a,b) for the 3-D reconstruction. Experimental B factors and defocus values for each CCD frame were estimated using a synthetic 1-D structure factor generated using the boxed out particles from several CCD frames as described in the *EMAN* documentation. The reconstruction run was instructed to use the far from focus images for the initial orientation parameter search and the close to focus images to refine the orientation parameters at higher resolution. Unique particles (6465) from the close to focus images were input into the final reconstruction (Table 1). Once the orientation parameters for each particle were determined, the 3-D map was generated using the Fourier Bessel inversion algorithm (Crowther, 1971; Zhou et al., 1998). The reconstruction required approximately 45 h on 16 AMD Athlon XP 1900+ processors.

2.8. Segmentation and analysis of 3D reconstruction

An asymmetric unit and single protein subunits were segmented from the final reconstruction using the template maps from the previous reconstruction of the same virus (Zhou et al., 2003). Each template was docked into the finished map using the program *foldhunter* (Jiang et al., 2001a,b). After being docked into the reconstruction, each template was converted into a binary mask. The binary mask was enlarged by several pixels to ensure that the subunit would not be truncated by the mask. This mask was then applied to the raw density map output from the 3-D reconstruction, resulting in a

segmented subunit. Each of the previous two steps was performed using the *EMAN* program *proc3d* (Ludtke et al., 1999). Segmented subunits and the template subunits were analyzed using the program *helixhunter* to estimate which regions of the map are most similar to a prototypical α -helix (Jiang et al., 2001a,b). Helix RMSD values were calculated using the program *DEJAVU* (Kleywegt and Jones, 1997). Rendering of CPV was done using *IRIS Explorer* (Numerical Algorithms Group, Oxford, UK) and a number of custom modules (*SAIL*) written for *IRIS Explorer* developed at the NCMI (Dougherty and Chiu, 2000). Visualization of the CSP-A subunit, with annotated α -helices, was done using the *Dino3D* software package (Philippson, 2003).

3. Results

3.1. CCD characterization and estimation of the CCD MTF at 200 kV

The performance of our CCD camera was evaluated in three ways. First, we examined images of graphite at

an effective magnification of $111\,000\times$ magnification. As shown in Fig. 1, the Fourier transform of a graphite image at this magnification clearly shows a peak at $1/3.44\text{ \AA}^{-1}$ corresponding to the spacing in graphite's reciprocal lattice. For an evaluation using a non-crystalline sample, we recorded images of amorphous carbon film and estimated the corresponding 2-D and 1-D power spectra (Fig. 2A–D). SNR as a function of spatial frequency can be estimated from these power spectra (Fig. 2E). The SNR plots that we calculated appear somewhat noisy in comparison to similar figures that we have published in the past (Saad et al., 2001). This is primarily because we are plotting the raw SNR curve rather than a fitted SNR curve that represents the data. In this comparison, the SNR of the CCD data is better than the SNR of the photographic film data at low spatial frequencies. At $2/5$ Nyquist frequency the SNR between the two datasets is equivalent and at higher spatial frequencies the SNR of film data is better than the SNR of CCD data. A similar trend was observed for images taken at different defocus values. Subsequently, the same experiment was performed over the same area of carbon film at a microscope magnification of

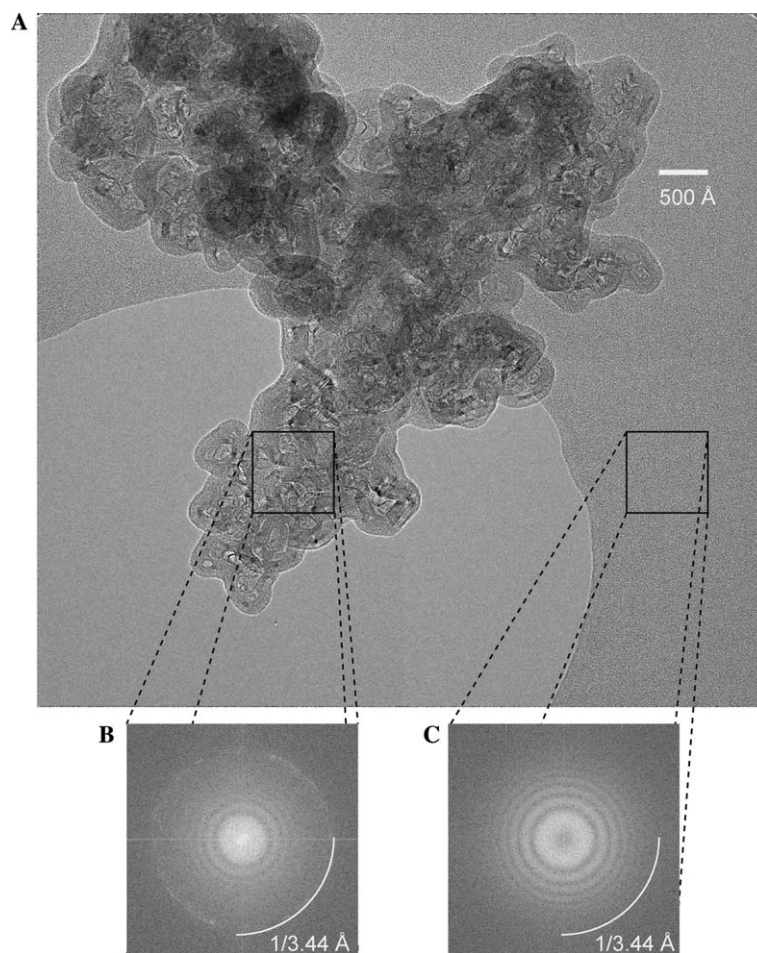


Fig. 1. Evaluation of the $4\text{k}\times 4\text{k}$ CCD camera at 200 kV on graphite. (A) Image of graphite acquired at $111\,000\times$ magnification on CCD. (B) Fourier transform of graphite from the image acquired in (A). (C) Fourier transform of amorphous carbon taken from the image acquired in (A).

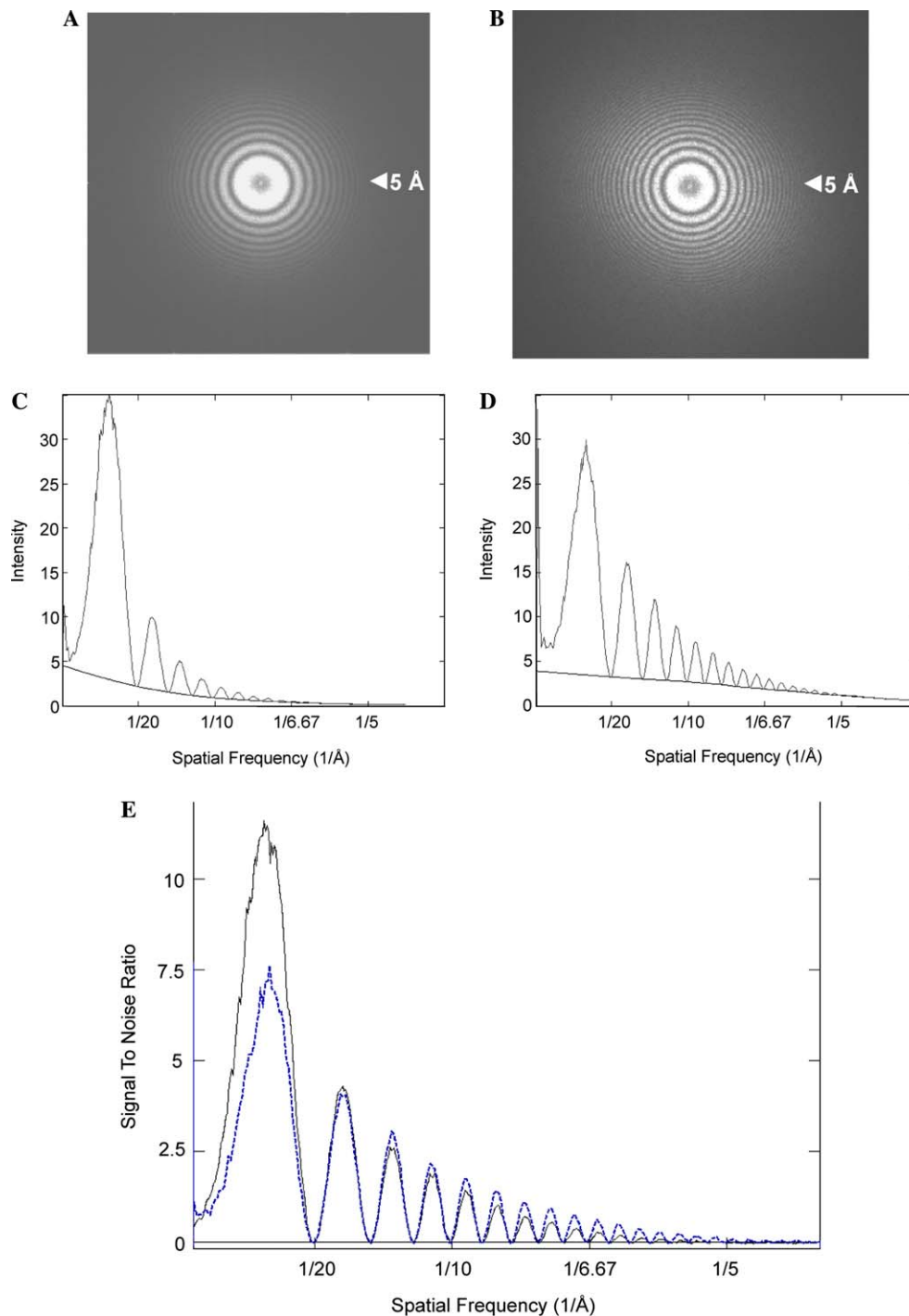


Fig. 2. Characterizing the CCD Camera. Images of amorphous carbon film recorded on CCD and photographic film followed by digitization in a Zeiss scanner. (A) 2-D power spectrum calculated from amorphous carbon film imaged on CCD. (B) 2-D power spectrum calculated from amorphous carbon film imaged with photographic film and scanned using a Zeiss scanner at 7 μm . (C–D) 1-D power spectrum and noise profile estimate calculated by rotationally averaging (A) and (B), respectively, and fitting a line through the zeroes of the contrast transfer function. Signal-to-noise ratio (SNR) comparison between images of amorphous carbon film collected on CCD and film is shown in (E). In a solid line is the SNR calculated from data collected on CCD. Shown in a dotted line is the SNR calculated from digitized data collected on film.

80 000 \times . The analysis showed the same trend regardless of microscope magnification. Finally, we confirmed our SNR comparison results by estimating the MTF function associated with the CCD camera by the noise method shown in Fig. 3 (de Ruijter and Weiss, 1992).

We measured the MTF using several different image dosages as specified in Section 2 within the range typically used for single particle imaging. At these dosage levels, we did not see any change in the MTF of the CCD camera.

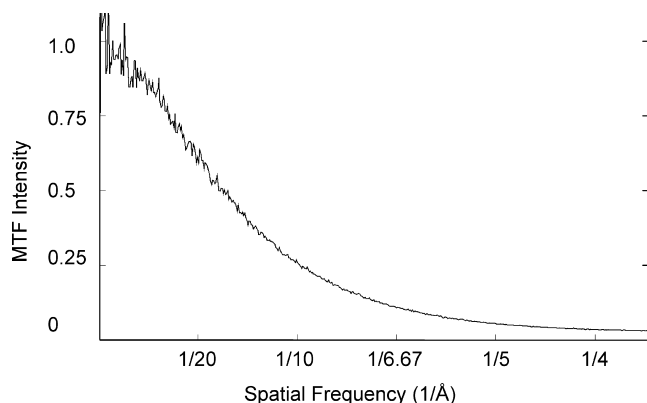


Fig. 3. Estimating the MTF of the CCD Camera. The CCD was evenly illuminated in the absence of sample to collect images of white noise which were used to estimate the MTF using the Noise method of (de Ruijter and Weiss, 1992).

3.2. Electron cryomicroscopy and analysis of ice embedded specimens

A total of 428 focal pairs of ice embedded CPV were acquired at 200 kV on our Gatan US4000 camera. Figs. 4A and B are 1/4 of the area of typical focal pair images of CPV recorded at 1.2 and 3.5 μm defocus, respectively. Data quality were estimated by approximating the fall-off of the contrast transfer function (CTF) rings with a Gaussian function described by a single parameter called an “experimental B factor.” Experimental B factors and defocus values for each CCD frame were estimated as described previously (Ludtke et al., 1999; Saad et al., 2001). The 2-D power spectrum (Figs. 4C and D) and its 1-D profile were used to estimate defocus, experimental B factor and noise parameters for each CCD frame. Finally, the quality of each frame was determined from the SNR plot from all the boxed particles (Figs. 4E and F). Each frame contained approximately 17 boxed particles and those particles that showed noticeable drift or astigmatism were excluded from further processing. Boxed particles, focal pair information, defocus and experimental B factor information were collected and provided to the SAVR software package for reconstruction (Jiang et al., 2001a,b).

3.3. Single particle reconstruction and refinement statistics

The effective resolution of the final 3-D reconstruction (Fig. 5) was 9 Å based on the 0.5 cut-off of the fourier shell correlation (FSC) between two reconstructions generated from half the data set (Fig. 6B) (Böttcher et al., 1997; Van Heel, 1987). One interesting statistic is the relatively high percentage (~86%) of the particles included in the final reconstruction from the set of boxed out particles provided to SAVR (Fig. 6A).

3.4. Structural features

An asymmetric unit of CPV is made up of 3 distinct polypeptides: one copy of TP, two copies of the CSP proteins (CSP-A and CSP-B), and two copies of the LPP proteins (LPP-3 and LPP-5). The CSP proteins share the same sequence, but are different structurally; this is also true for the LPP proteins. Fig. 7 illustrates how well these secondary structure elements were resolved in one of the five capsid shell protein (CSP-A). As shown previously (Böttcher et al., 1997; Chiu et al., 2002; Conway et al., 1997), an α -helix at this resolution appears to be like a “sausage” with a ~ 6 Å diameter at an appropriate contour level. Several vertical helices in the apical domain and a number of transverse helices in the carapace domain are visible. The dimerization domain contains several potential β -sheets regions, with a few scattered helices. This secondary structure element organization bears a similarity to that of the orthoreovirus $\lambda 1$ capsid protein (Reinisch et al., 2000).

3.5. Comparison of CPV reconstruction with other structures

We compared the results of our reconstruction from data collected entirely on CCD with a previous 8 Å reconstruction from images collected on photographic film (Zhou et al., 2003). A visual comparison between these two maps showed that the two reconstructions were almost identical. We quantified this observation in two ways. First, we determined that the spatial frequency at which the FSC between the two maps fell below 0.5 was at $1/9 \text{ \AA}^{-1}$ resolution (Fig. 6C). Second, we compared the centroid positions of the α -helices identified in CSP-A and CSP-B (Table 2). The average RMSD between common helices found in these two maps is 2.5 Å for CSP-A and 1.9 Å for CSP-B. The RMSD values between the helices in the CSP proteins from our reconstruction and the corresponding proteins from orthoreovirus $\lambda 1$ (1EJ6-B and 1EJ6-C) (Reinisch et al., 2000) are less than 5 and 6.5 Å, respectively (Table 2).

4. Discussion

CCD cameras offer a number of significant advantages over film as a recording media for electron cryomicroscopy. The broad dynamic range, high linearity, and low level of noise make these devices ideal for recording diffraction intensities of 2-D crystals (Faruqi and Subramaniam, 2000). A CCD camera gives instant feedback to the microscopist on the quality of the data being collected and can reduce time spent collecting inferior data due to poor quality of the frozen hydrated specimen or suboptimal microscope conditions. The absence of photographic film in the microscope vacuum significantly

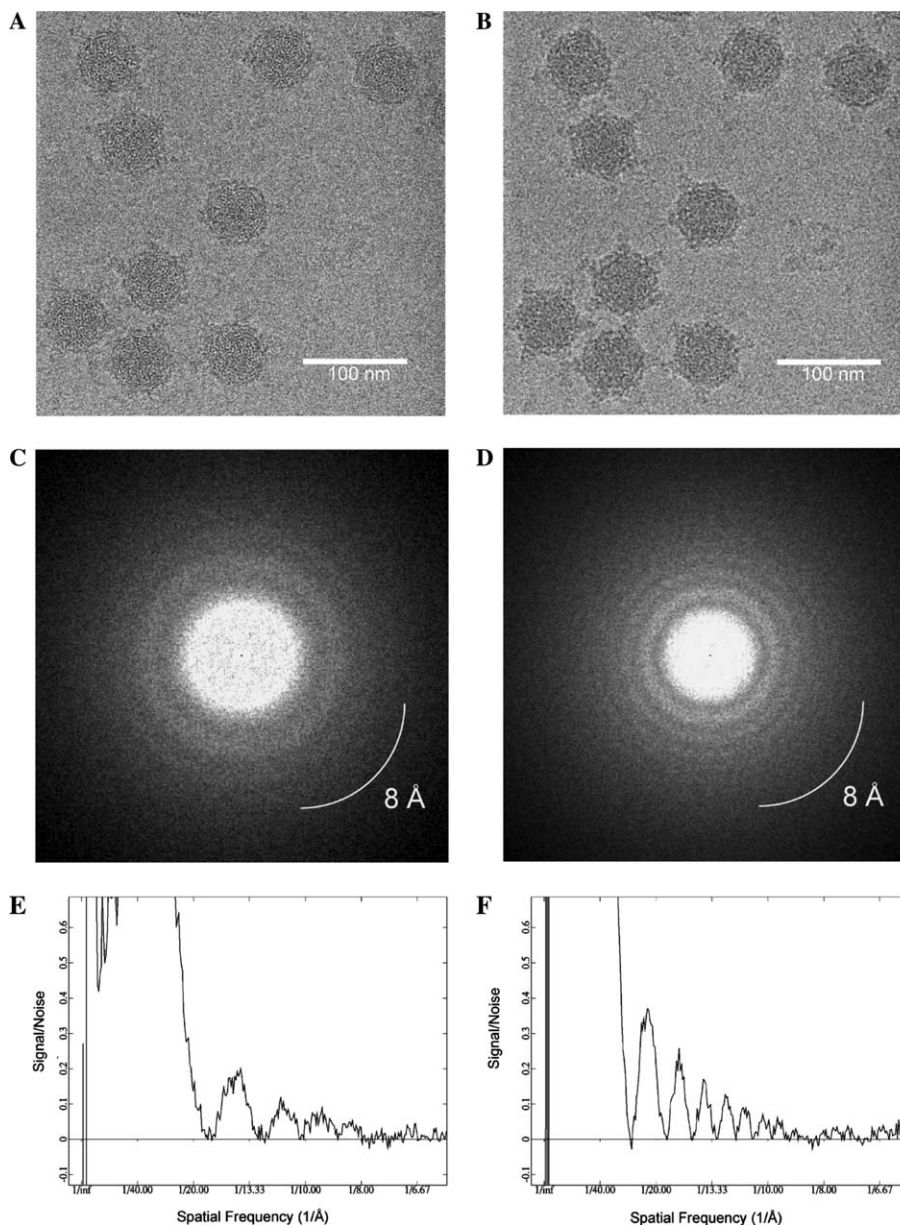


Fig. 4. Focal pair of images and data quality analysis of ice embedded cytoplasmic polyhedrosis virus (CPV). (A,B) Raw CCD images of ice embedded CPV taken at 1.2 μm underfocus (A) and 3.5 μm underfocus (B). Images in (A) and (B) show approximately one quarter of the total area of the CCD frame. 2-D Power spectra calculated from the particles in (A) and (B) are shown in (C) and (D), respectively. SNR from the power spectra in (C) and (D) are shown in (E) and (F), respectively.

extends the usable time of a cryo-EM grid during a microscope session without noticeable ice contamination as photographic film absorbs a significant amount of water even though they are thoroughly evacuated prior to use in the microscope. We have noted the feasibility of using the same ice-embedded specimen grid continuously for more than two days without noticeable contaminant buildup on the sample. Most importantly, the 4 k \times 4 k CCD camera appears to have partially overcome the limitations of previous CCD cameras and is capable of imaging ice embedded biological specimens to subnanometer resolution, as we have described here.

4.1. CCD characterization

The first test of the 4 k \times 4 k CCD camera appeared promising, as evidenced by the visualization of the graphite lattice at relatively low magnification (Fig. 1). This showed that with strong enough signal, information at 4/5 Nyquist frequency could be detected.

To examine the performance of the CCD camera at all spatial frequencies, we examined images of amorphous carbon collected on the CCD camera. Amorphous carbon is a suitable test specimen since it has a scattering power similar to biological samples while not

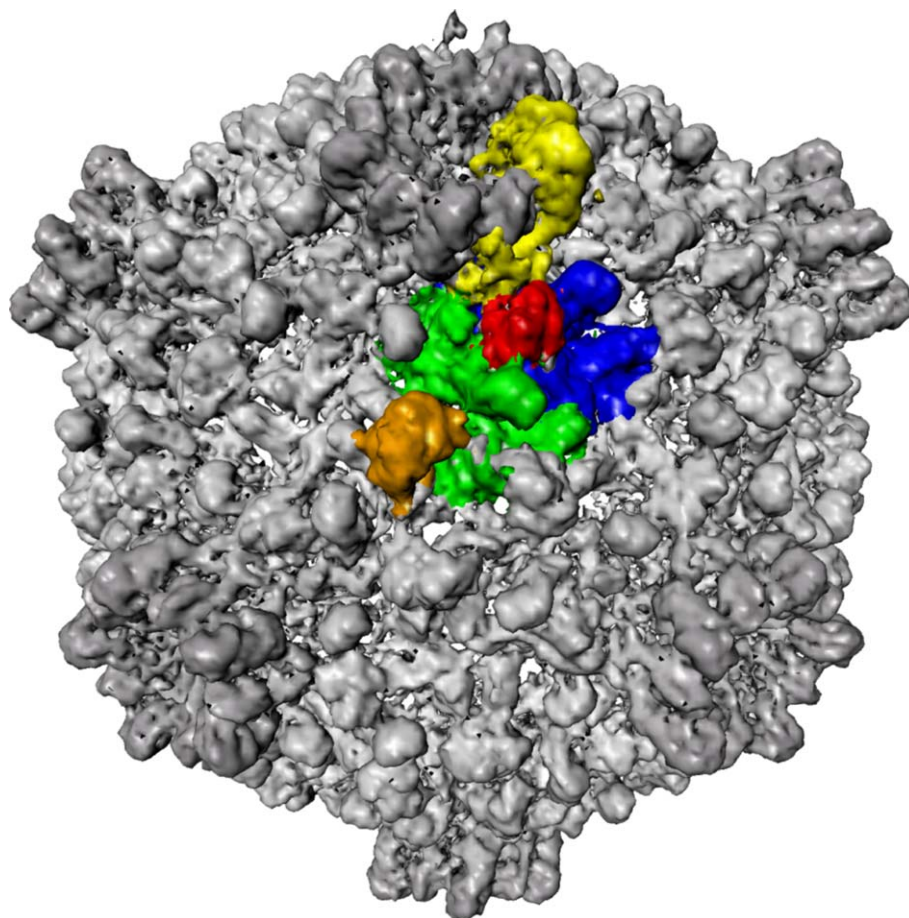


Fig. 5. Visualizing the asymmetric unit of cytoplasmic polyhedrosis virus (CPV). A 3-fold view of the virus. The proteins in the asymmetric unit are coloured as follows: CSP-A (blue), CSP-B (green), LPP-3 (red), LPP-5 (orange), and TP (yellow).

showing the same kind of beam sensitivity that real biological samples exhibit. Fig. 2E shows that the SNR between data collected on CCD and film is very similar up to $2/5$ Nyquist frequency. In this analysis, one may be concerned with the effect on the SNR estimate due to different sampling intervals and the total sampling area on the detectors. For instance, the CCD camera had a sampling value of $1.81 \text{ \AA}/\text{pixel}$, while the film data has a value of $1.17 \text{ \AA}/\text{pixel}$. This difference is caused by the different locations of the film and the CCD in the microscope column. However, we have observed that the SNR is governed by the electron dosage per unit area at the specimen. The image size only affects the smoothness of the power spectrum and thus the smoothness of the SNR. The difference in sampling ($\text{\AA}/\text{pixel}$) values is the same as applying a low pass filter to the image with the larger $\text{\AA}/\text{pixel}$ and will not effect on the SNR as long as the SNR is zero at Nyquist frequency. In our case, the total power decays to less than 2.5% at Nyquist frequency so that the effect of aliasing at $2/5$ Nyquist frequency is negligible.

Furthermore, we employed a convenient method (de Ruijter and Weiss, 1992) to assess the MTF of the CCD camera. It has been previously described that this

method will not yield the most accurate estimate of the “true” MTF function of the CCD camera (Ishizuka, 1993; Meyer and Kirkland, 2000; van Zwet and Zandbergen, 1996). Nevertheless, this type of analysis is widely used. Furthermore, when coupled with our SNR comparison with photographic film, this measurement has provided adequate estimate for setting a practically attainable resolution in structural determination by single particle reconstruction. For the CPV data collection, we chose an effective magnification of $83\,100\times$ in order to retrieve at least 9 \AA structural information which is expected to fall below $2/5$ Nyquist frequency.

It is interesting to compare our results with those obtained using a similar camera at 120 kV (Zhang et al., 2003). First, both studies reported seeing the 3.44 \AA^{-1} peak in the Fourier transform of graphitized carbon at similar magnification ($71,000\times$ magnification at 120 kV and $83\,100\times$ magnification at 200 kV). Second, we both observed that the SNR from images of amorphous carbon detected on film and CCD look very similar up to the $2/5$ Nyquist frequency region. One would expect the camera to perform better at 120 kV than at 200 kV. The fact that the results are similar despite the difference in accelerating voltages is likely due to the partial spatial

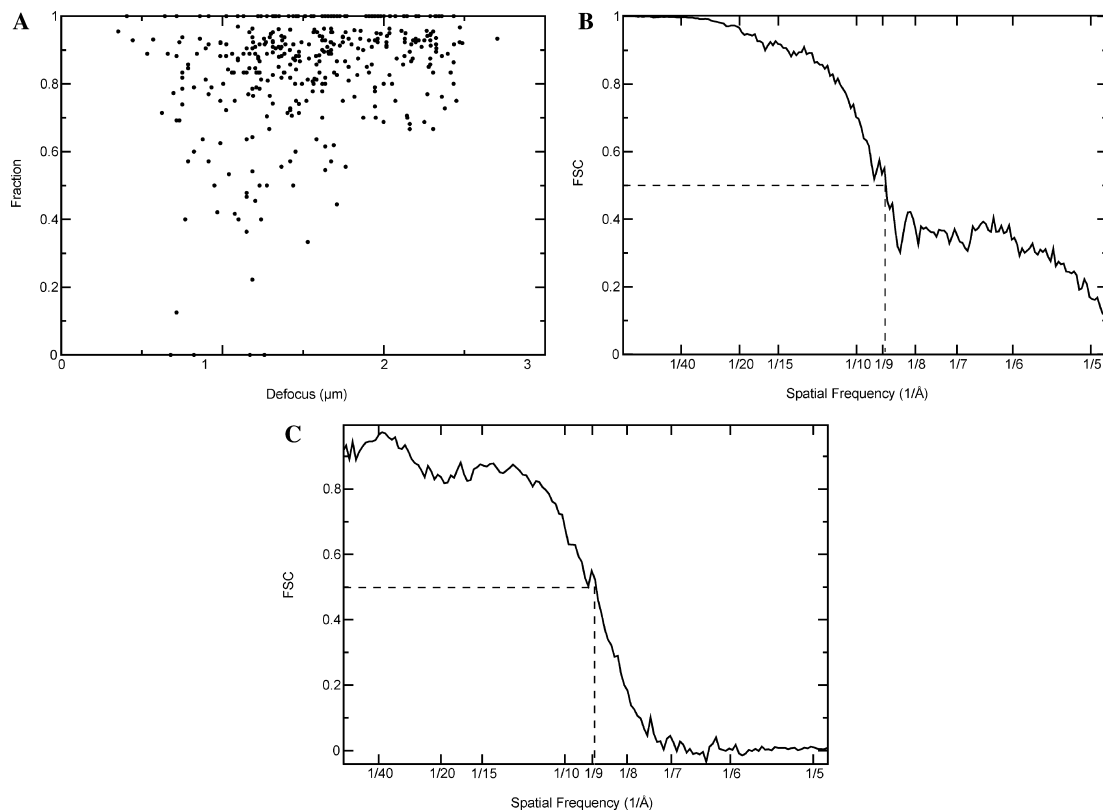


Fig. 6. Refinement statistics for CPV reconstruction. Shown in (A) is the fraction of particles included in the final reconstruction from each CCD frame. (B,C) Two estimates of the resolution of the final 3-D reconstruction. The estimate in (B) shows the Fourier Shell Correlation (FSC) between two reconstructions generated from half of the data collected on CCD. The resolution estimate in (C) shows the FSC between our final reconstruction and the final reconstruction from previous structure.

coherence of the tungsten filament as an electron source in the 120 kV study.

4.2. Imaging ice embedded virus particles

Previous work has indicated that CCD cameras may be used successfully to collect data of ice embedded single particles for 3-D reconstructions at relatively low resolution ($\sim 14\text{--}30\text{ \AA}$) and low accelerating voltage (100–120 kV) (Faruqi and Subramaniam, 2000; Rouiller et al., 2001; Stewart et al., 2000; Zhang et al., 2003). These works demonstrated that, even with a smaller imaging area, these cameras can be employed to collect data for a biologically relevant reconstruction. What remained unknown was whether or not these cameras may be used to reach sub-nanometer resolution by cryo-EM and single particle reconstruction techniques, and how severe the effect on the MTF will be by moving up to 200 kV. We addressed these questions in a practical manner by determining the CPV structure to 9 \AA .

The data collection for this project took a total of 5 days, corresponding to about 85 focal pairs per day. Through the course of this project, and subsequent projects, we developed software tools, to make the data collection more efficient, allowing us to acquire ~ 200

focal pairs a day or ~ 400 frames per day (data unpublished). That is to say, a single grid over a period of two days of data collection is adequate to collect the data set reported here, provided that the specimen can be prepared with appropriate particle distribution. The details of software developments will be described in more detail in a subsequent publication.

The SNR of our image data (Fig. 4A–F) clearly extends beyond 9 \AA^{-1} . It is also evident from these images that the particles have much higher contrast than similarly defocused images acquired on film (unpublished observation). Examination of the SNR plots of Fig. 2E led to the same observation. The SNR of low frequency information, largely responsible for the contrast of particle in an image, is much higher from CCD collected data than on film. We observed that the CCD camera acts as both an amplifier and a low pass filter. The scintillator acts as an amplifier, producing 20–30 photons for every incident electron increasing the SNR. The drawback, however, is that these photons are not localized to the point at which the electron entered the scintillator, increasing the point spread function. This results in two contradictory effects; increasing the SNR at low frequency while attenuating the SNR at higher spatial frequency. The combinatory effect of these factors makes the SNR of CCD data better than

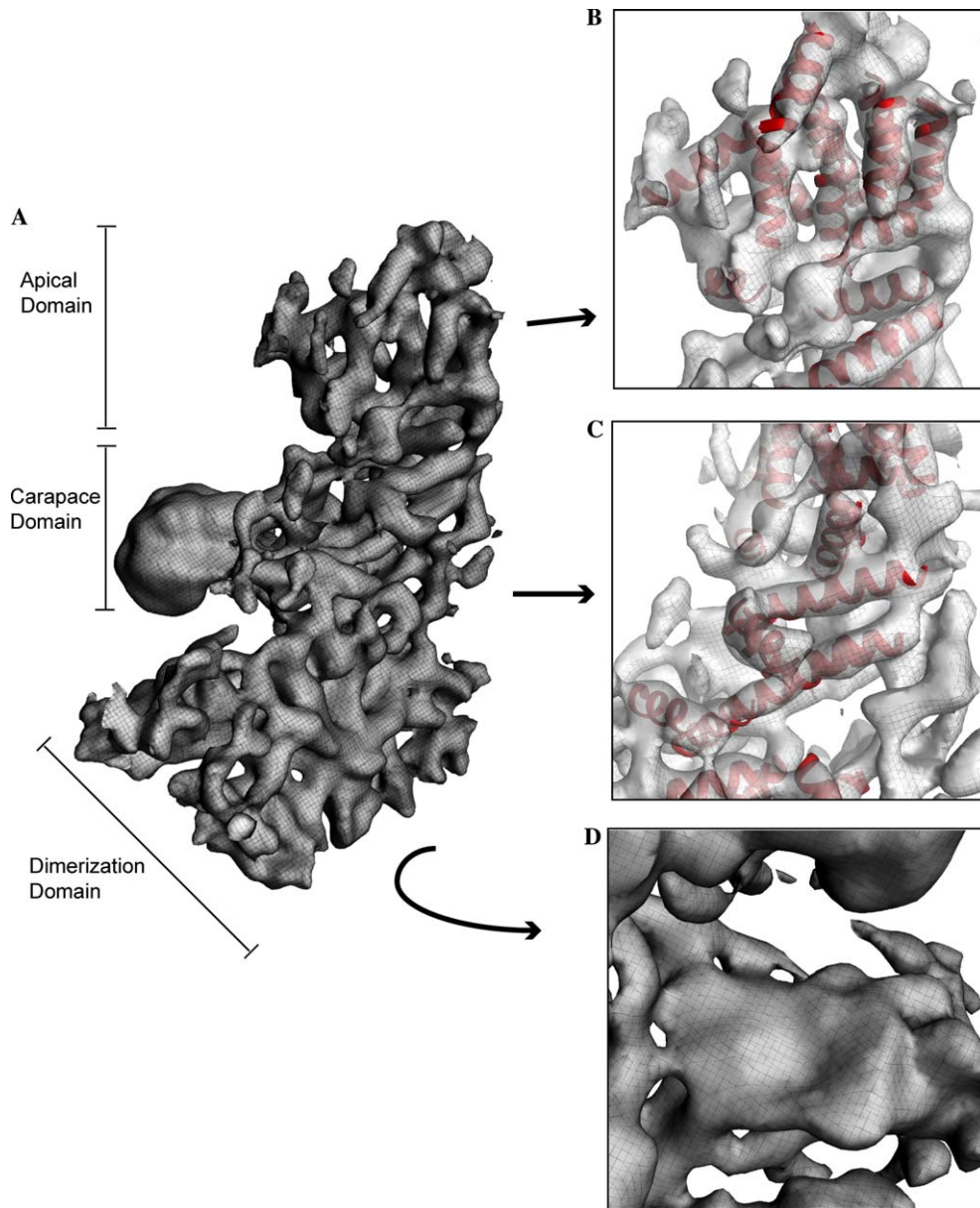


Fig. 7. Visualizing α -helices and putative β -sheets from the final reconstruction of cytoplasmic polyhedrosis virus (CPV). *Helixhunter* was used to estimate the density in the map that corresponds to alpha helices in this protein; the red coils indicate the region that is predicted to correspond to these helices. Shown is the CSP-A subunit from the CPV capsid (A). (B,C) The apical and carapace domains of CSP-A, respectively. An image of the dimerization domain of CSP-A rotated by 180° is shown in (D). This is a broad flat region that we have putatively called a β -sheet.

film data at low spatial frequency while being attenuated at high spatial frequency.

4.3. Sub-nanometer resolution structure

Using the relatively conservative 0.5 FSC criterion, we estimate the effective resolution of our map to be 9 Å (Fig. 6B). This is the highest resolution achieved to date by electron cryomicroscopy and single particle reconstruction techniques using data collected on a CCD camera. An interesting observation from this reconstruction was the relatively large percentage yield of particles that were included in the final reconstruct-

tion, likely reflecting the better low resolution contrast of the CCD images. This would aid in the accurate boxing and 2-D alignment of these particles allowing their orientation and center to be more accurately determined.

4.4. Comparison of CCD based reconstruction and other related structures

The ultimate practical method for comparing CCD to film as a method for data collection is a direct comparison of this reconstruction with a previous reconstruction collected on film. The 0.5 FSC criterion between these

Table 2
Evaluation of the reliability of the α -helices found from this reconstruction

Component	CSP-A (RMSD)	CSP-B (RMSD)
RMSD with previous CPV map (Zhou et al., 2003)	2.50 (16 helices)	1.92 (12 helices)
RMSD with 1EJ6-B	4.69 (11 of 25 helices)	5.48 (8 of 25 helices)
RMSD with 1EJ6-C	4.43 (11 of 30 helices)	6.35 (9 of 30 helices)

Helices identified in this reconstruction were compared to helices that could be identified from the previous reconstruction of CPV (row 1) at 8 Å (Zhou et al., 2003). Shown in rows 2 and 3 are the average RMSD values for helices found in this map and helices greater than 6 residues in length described in the *orthoreovirus* capsid proteins crystal structure.

two maps provided an independent confirmation of our resolution estimate of 9 Å resolution (Fig. 6C).

As a final test of the reliability of the map, we judged the detection of the α -helices and compared them to the equivalent α -helices generated from the previous cryo-EM reconstruction and also to the homologous reovirus protein $\lambda 1$ (1EJ6-B and 1EJ6-C) solved by X-ray crystallography. Table 2 shows the RMSD values calculated between the α -helices in these structures and those found in our map. The α -helices found from Zhou's structure differed from our map by less than 2.5 Å. These differences are likely due to the slightly different methods of handling the contrast transfer function and B factor compensation. However, the two maps look basically the same. In addition, reovirus $\lambda 1$ and the CPV CSP proteins showed between 4.4 and 6.35 Å RMSD between the α -helices in these two proteins even though the proteins from the two viruses have less than 10% in sequence identity. As *helixhunter* can only detect α -helices longer than 3 turns, only one third of these helices had a corresponding helix in the CPV CSP maps. Given this relatively high RMSD between the two viruses at this resolution, they appear to have non-identical protein folds though the overall helical organization is quite similar. Such structural similarity has also been observed between the crystal structures of reovirus and bluetongue virus in the same virus family (Grimes et al., 1998; Reinisch et al., 2000).

5. Conclusions

A 1 k × 1 k CCD camera has been shown to be capable of imaging protein crystals beyond 4 Å resolution with a 400 kV cryomicroscope (Sherman and Chiu,

1997; Sherman et al., 1996). In this work we have for the first time demonstrated that a CCD camera in a 200 kV cryomicroscope can be used for collecting images useful for determining the structure of a non-crystalline sample at sub-nanometer resolution. We show that for a microscope operating at 200 kV, the MTF of the camera, while still a limiting factor, allows reconstructions almost as good as those produced from data sets collected on photographic film. Finally, the reconstruction produced from a dataset acquired entirely on CCD can accurately reproduce the structure of the macromolecule being imaged.

Film continues to provide greater SNR at spatial frequencies greater than 2/5 Nyquist frequency and a larger field of view than the CCD camera, necessary for collecting the quality and quantity of data necessary for structures at better than 9 Å resolution. We believe that the CCD cameras can provide images suitable for reconstruction beyond 9 Å. Obviously, higher resolution structures require more and higher quality images. As the MTF of the CCD camera appears to be limiting the structural resolution under the current imaging conditions, there are two ways to improve the resolution of the reconstruction. As shown in Fig. 4E, there is still detectable signal beyond 1/9 Å⁻¹ in our image data, though the SNR is relatively low. It is conceivable that one could use more particles to build up statistics in order to retrieve structural information beyond 2/5 Nyquist frequency. This would require a more powerful image reconstruction algorithm. Alternatively, one can use a higher magnification, so that 2/5 Nyquist frequency would correspond to a higher spatial frequency value. As shown in Table 3, a structure out to 1/6.7 Å⁻¹, which is equivalent to 2/5 Nyquist frequency, should be possible if imaging is done at an effective magnification of 11 04 000 ×. However, this

Table 3
Relationship of effective microscope magnification, sampling value, specimen area and 2/5 Nyquist frequency relative to those at 82 800 × magnification

Effective Microscope magnification	Å/pix	Dimension of CCD frame on specimen (nm)	CCD frame area compared to 82 800 (%)	2/5 Nyquist (Å)
55 200	2.71	1110	225.00%	13.55
69 000	2.17	886	144.00%	10.84
82 800	1.81	738	100.00%	9.03
1 10 400	1.35	554	56.25%	6.77
1 38 000	1.08	443	36.00%	5.42
2 07 000	0.72	295	16.00%	3.61

later approach would result in 50% less area and thus fewer particles per CCD frame. In either approach, one would need many times more data. An automated image acquisition would definitely make such a process simpler (Carragher et al., 2004).

Acknowledgments

This research has been supported by NIH Grants (P41RR02250, R21AI053737, R01AI38469, R01AI46420, and R01CA94809), Robert Welch Foundation (to CRB), Agouron Institute (to WJ) and the NLM training Grant (T15LM07093 to MLB) through W. M. Keck Center of the Gulf Coast Consortia. We thank Joanita Jakana and Michael Marsh for helpful assistance and discussion and Xuekui Yu and Jing-qiang Zhang in providing the CPV sample.

References

- Aikens, R., Agard, D.A., 1989. Solid-state imagers for microscopy. *Methods Cell Biol.* 29, 291–313.
- Böttcher, B., Wynne, S.A., Crowther, R.A., 1997. Determination of the fold of the core protein of hepatitis B virus by electron cryomicroscopy. *Nature* 386, 88–91.
- Carragher, B., Fellmann, D., Guerra, F., Milligan, R.A., Mouche, F., Pulokas, J., Sheehan, B., Quispe, J., Suloway, C., Zhu, Y., Potter, C.S., 2004. Rapid routine structure determination of macromolecular assemblies using electron microscopy: current progress and further challenges. *J. Synchrotron. Radiat.* 11, 83–85.
- Chiu, W., Baker, M.L., Jiang, W., Zhou, Z.H., 2002. Deriving folds of macromolecular complexes through electron cryomicroscopy and bioinformatics approaches. *Curr. Opin. Struct. Biol.* 12, 263–269.
- Conway, J.F., Cheng, N., Zlotnick, A., Wingfield, P.T., Stahl, S.J., Steven, A.C., 1997. Visualization of a 4-helix bundle in the hepatitis B virus capsid by cryo-electron microscopy. *Nature* 386, 91–94.
- Crowther, R.A., 1971. Procedures for three-dimensional reconstruction of spherical viruses by Fourier synthesis from electron micrographs. *Philos. Trans. R. Soc. Lond. B. Biol. Sci.* 261, 221–230.
- de Ruijter, W.J., Weiss, J.K., 1992. Methods to measure properties of slow-scan CCD cameras for electron detection. *Rev. Sci. Instrum.* 63, 4314–4321.
- Dougherty, M., Chiu, W., 2000. Macromolecular structure visualization tools at NCM. *Microsc. Microanal.* 6, 282–283.
- Downing, K.H., Hendrickson, F.M., 1999. Performance of a 2k CCD camera designed for electron crystallography at 400 kV. *Ultramicroscopy* 75, 215–233.
- Faruqi, A.R., Subramaniam, S., 2000. CCD detectors in high-resolution biological electron microscopy. *Q. Rev. Biophys.* 33, 1–27.
- Grimes, J.M., Burroughs, J.N., Gouet, P., Diprose, J.M., Malby, R., Zientara, S., Mertens, P.P., Stuart, D.I., 1998. The atomic structure of the bluetongue virus core. *Nature* 395, 470–478.
- Ishizuka, K., 1993. Analysis of electron image detection efficiency of slow-scan CCD cameras. *Ultramicroscopy* 52, 7–20.
- Jiang, W., Baker, M.L., Ludtke, S.J., Chiu, W., 2001a. Bridging the information gap: computational tools for intermediate resolution structure interpretation. *J. Mol. Biol.* 308, 1033–1044.
- Jiang, W., Li, Z., Zhang, Z., Booth, C.R., Baker, M.L., Chiu, W., 2001b. Semi-automated icosahedral particle reconstruction at subnanometer resolution. *J. Struct. Biol.* 136, 214–225.
- Kivioja, T., Ravantti, J., Verkhovsky, A., Ukkonen, E., Bamford, D., 2000. Local average intensity-based method for identifying spherical particles in electron micrographs. *J. Struct. Biol.* 131, 126–134.
- Kleywegt, G.J., Jones, T.A., 1997. Detecting folding motifs and similarities in protein structures. Academic Press, London.
- Ludtke, S.J., Baldwin, P.R., Chiu, W., 1999. EMAN: semiautomated software for high-resolution single-particle reconstructions. *J. Struct. Biol.* 128, 82–97.
- Ludtke, S.J., Jakana, J., Song, J.L., Chuang, D.T., Chiu, W., 2001. A 11.5 Å single particle reconstruction of GroEL using EMAN. *J. Mol. Biol.* 314, 253–262.
- Ludtke, S.J., Nason, L., Tu, H., Peng, L., Chiu, W., 2003. Object oriented database and electronic notebook for transmission electron microscopy. *Microsc. Microanal.* 9, 556–565.
- Meyer, R.R., Kirkland, A.I., 2000. Characterisation of the signal and noise transfer of CCD cameras for electron detection. *Microsc. Res. Tech.* 49, 269–280.
- Philippson, A., 2003. Dino: Visualizing Structural Biology. Available from <http://www.dino3d.org>. 2003.
- Reinisch, K.M., Nibert, M.L., Harrison, S.C., 2000. Structure of the reovirus core at 3.6 Å resolution. *Nature* 404, 960–967.
- Rouiller, I., Pulokas, J., Butel, V.M., Milligan, R.A., Wilson-Kubalek, E.M., Potter, C.S., Carragher, B.O., 2001. Automated image acquisition for single-particle reconstruction using p97 as the biological sample. *J. Struct. Biol.* 133, 102–107.
- Saad, A., Ludtke, S.J., Jakana, J., Rixon, F.J., Tsuruta, H., Chiu, W., 2001. Fourier amplitude decay of electron cryomicroscopic images of single particles and effects on structure determination. *J. Struct. Biol.* 133, 32–42.
- Sherman, M.B., Brink, J., Chiu, W., 1996. Performance of a slow-scan CCD camera for macromolecular imaging in a 400 kV electron cryomicroscope. *Micron* 27, 129–139.
- Sherman, M.B., Chiu, W., 1997. Reliability of phases retrieved from 400-kV spot-scan images of purple membranes acquired on a slow-scan CCD camera. *J. Microsc.* 188 (Pt 3), 285–289.
- Stewart, P.L., Cary, R.B., Peterson, S.R., Chiu, C.Y., 2000. Digitally collected cryo-electron micrographs for single particle reconstruction. *Microsc. Res. Technol.* 49, 224–232.
- Van Heel, M., 1987. Angular reconstitution: a posteriori assignment of projection directions for 3D reconstruction. *Ultramicroscopy* 21, 111–123.
- van Zwet, E.J., Zandbergen, H.W., 1996. Measurement of the modulation transfer function for a slow-scan CCD camera on a TEM using a thin amorphous film as a test signal. *Ultramicroscopy* 64, 49–55.
- Zhang, P., Borgnia, M.J., Mooney, P., Shi, D., Pan, M., O'Herron, P., Mao, A., Brogan, D., Milne, J.L., Subramaniam, S., 2003. Automated image acquisition and processing using a new generation of 4k × 4k CCD cameras for cryo electron microscopic studies of macromolecular assemblies. *J. Struct. Biol.* 143, 135–144.
- Zhou, Z.H., Chiu, W., 2003. Determination of icosahedral viruse structure by electron cryomicroscopy at subnanometer resolution. *Adv. Protein Chem.* 64, 93–124.
- Zhou, Z.H., Chiu, W., Haskell, K., Spears Jr., H., Jakana, J., Rixon, F.J., Scott, L.R., 1998. Refinement of herpesvirus B-capsid structure on parallel supercomputers. *Biophys. J.* 74, 576–588.
- Zhou, Z.H., Zhang, H., Jakana, J., Lu, X.Y., Zhang, J.Q., 2003. Cytoplasmic polyhedrosis virus structure at 8 Å by electron cryomicroscopy: structural basis of capsid stability and mRNA processing regulation. *Structure (Camb)* 11, 651–663.